Large-area display textiles integrated with functional systems

Huisheng Peng (penghs@fudan.edu.cn)
Fudan University https://orcid.org/0000-0002-2142-2945

Xiang Shi
Fudan University

Yong Zuo
Fudan University

Peng Zhai
Fudan University

Jiahao Shen
Fudan University

Yangyiwei Yang
Technische Universität Darmstadt

Zhen Gao
Fudan University

Meng Liao
Fudan University

Jiawei Wang
Fudan University

Xiaojie Xu
Fudan University

Qi Tong
Fudan University

Bo Zhang
Fudan University https://orcid.org/0000-0002-7853-979X

Xuemei Sun
State Key Laboratory of Molecular Engineering of Polymers, Department of Macromolecular Science and Laboratory of Advanced Materials, and Department of Chemistry, Fudan University
https://orcid.org/0000-0002-2583-8593

Lihua Zhang
Fudan University

Qibing Pei
University of California, Los Angeles https://orcid.org/0000-0003-1669-1734

Dayong Jin

University of Technology Sydney https://orcid.org/0000-0003-1046-2666

Peining Chen

Fudan University

Research Article

Keywords: textiles, electronic devices, fabrication

Posted Date: August 17th, 2020

DOI: https://doi.org/10.21203/rs.3.rs-56463/v1

Version of Record: A version of this preprint was published at Nature on March 10th, 2021. See the published version at https://doi.org/10.1038/s41586-021-03295-8.

Large-area display textiles integrated with functional systems

Xiang Shi[1†], Yong Zuo[1†], Peng Zhai[2†], Jiahao Shen[3], Yangyiwei Yang[4], Zhen Gao[1], Meng Liao[1], Jiawei Wang[1], Xiaojie Xu[1], Qi Tong[3], Bo Zhang[1], Xuemei Sun[1], Lihua Zhang[2], Qibing Pei[5], Dayong Jin[6], Peining Chen[1*], Huisheng Peng[1*]

[1]*State Key Laboratory of Molecular Engineering of Polymers, Department of Macromolecular Science and Laboratory of Advanced Materials, Fudan University, Shanghai, 200438, China.*

[2]*The Institute of AI and Robotics, Fudan University, Shanghai, 200433, China.*

[3]*Department of Aeronautics and Astronautics, Fudan University, Shanghai, 200433, China.*

[4]*Mechanics of Functional Materials Division, Institute of Materials Science, Technische Universität Darmstadt, Darmstadt, 64287, Germany.*

[5]*Department of Materials Science and Engineering, Henry Samueli School of Engineering and Applied Science, University of California Los Angeles, Los Angeles, CA, 90095, USA.*

[6]*Institute for Biomedical Materials & Devices (IBMD), School of Mathematical and Physical Sciences, Faculty of Science, University of Technology Sydney, NSW, 2007, Australia.*

Displays are basic building blocks of modern electronics[1,2]. Integrating displays into textiles offers exciting opportunities for smart electronic textiles – the ultimate form of wearables poised to change the way we interact with electronic devices[3-6]. Display textiles serve to bridge human-machine interactions[7-9], offering for instance, a real-time communication tool for individuals with voice or speech disorders. Electronic textiles capable of communicating[10], sensing[11,12] and supplying electricity[13,14] have been reported previously. However, textiles with functional, large-area displays have not been achieved so far because obtaining small illuminating units that are both durable and easy to assemble over a wide area is challenging. Here, we report a 6 m (L) × 25 cm (W) display textile containing 5×10^5 electroluminescent (EL) units narrowly spaced to ~800 μm. Weaving conductive weft and luminescent warp fibres forms micron-scale EL units at the weft-warp contact points. Brightness between EL units deviates by < 6.3% and remains stable even when the textile is bent, stretched or pressed. We attribute this uniform and stable lighting to the smooth luminescent coating around the

warp fibres and homogenous electric field distribution at the contact points. Our display textile is flexible and breathable and withstands repeatable machine-washing, making them suitable for practical applications. We show an integrated textile system consisting of display, keyboard and power supply can serve as a communication tool, which could potentially drive the Internet of Things in various areas including healthcare. Our approach unifies the fabrication and function of electronic devices with textiles, and we expect weaving fibre materials to shape the next-generation electronics.

Display devices have evolved from rigid panels to flexible thin films[15]. However, the configuration and fabrication of electronic textiles are different from conventional film devices such as organic light-emitting diodes (OLEDs) that are currently used to construct flexible displays. Textiles are woven from fibres, forming rough and porous structures that can deform and fit the contours of the human body[16,17]. OLEDs, on the other hand, are made by depositing multiple layers of semiconducting organic thin films between cathode and anode electrodes that are placed on planar substrates such as glass or plastic[18]. Depositing organic thin films on fibres that are suitable for weaving into flexible display textiles is very difficult because these thin films are too fragile to withstand the chafing during weaving. The evaporation method used to make OLEDs is not amenable to large-scale fabrication of fibre electrodes. More importantly, because light emission in OLEDs depends on carrier injection and transport between the anode and cathode[19,20], weaving warps and wefts cannot provide sufficient high quality ohmic contact between the electrodes and semiconducting layers for illumination.

In our study, we used electric-field driven devices based on ZnS phosphor to weave a display textile. Unlike OLED devices, ZnS phosphor dispersed in an insulating polymer matrix is activated by alternating electric field across polymer matrix[21]. Such electric-field driven devices require only spatial contacts between wefts and warps to illuminate[22,23], making them intrinsically durable and suitable for large-scale production. We prepared transparent (over 90% transmittance) conductive weft fibres by melt-spinning ionic-liquid-doped polyurethane gel (**Extended Data Fig. 1a-c**), and luminescent warp fibres by coating commercially available ZnS phosphor on silver-plated conductive yarn (**Extended Data Fig. 1d-f**). This solution-based coating presents a simple process to obtain luminescent warp fibres continuously. We chose polyurethane as polymer matrix because it is durable to friction, compression and bending during weaving. To ensure uniform coating of

ZnS, we dip-coated the conductive yarn in ZnS phosphor slurry and passed it through a home-made scraping micro-pinhole before drying (**Extended Data Fig. 2a**). The micro-pinhole smoothed the coating along the longitudinal and circumferential directions (**Extended Data Fig. 2b, c**). Different diameters of the micro-pinhole were used to tune the thickness of the ZnS phosphor layer. We used an optimized thickness of ~70 μm in our experiments unless specified otherwise. To evaluate the uniformity of the luminescent coating, we placed a 100-metre-long luminescent warp into salt water and applied alternating voltage between them (**Extended Data Fig. 2d**). The luminescence remained stable even when twisted (**Extended Data Fig. 2e**). For a 30-metre-long fibre, the luminescence intensity varied by less than 10% (**Extended Data Fig. 2f, g**). The intensity along the circumference at different locations of the fibre was almost identical and was independent of observation angle (**Extended Data Fig. 2h**). Fibres with an uneven ZnS phosphor coating (**Extended Data Fig. 2i**) showed uneven brightness and failure in some EL units (**Extended Data Fig. 2j, k**), indicating that light emission requires a uniform luminescent coating.

When the conductive weft and luminescent warp fibres are woven with cotton yarn using an industrial rapier loom, each interlaced weft and warp forms an effective EL unit (**Fig. 1a**, **Extended Data Fig. 1h, i**). Using this method, we produced a 6 m (L) × 25 cm (W) large-area display textile containing approximately 5×10^5 EL units (**Fig. 1b** and **Supplementary Movie 1**). The relative deviations of emission intensity for 600 EL units examined were narrowly between -6.3% to 5.2% (**Fig. 1c)**. Such small differences (< 10%) in intensity indicate that these fibres are well-suited for making large-area display textiles at scale (**Fig. 1d**). Even after 1,000 cycles of bending (**Fig. 1e**), stretching (**Fig. 1f**) and pressing (**Fig. 1g**), the intensity of these 600 EL units remained stable (with < 10% variations). We also obtained colourful textiles (**Fig. 1h**) with uniformly spaced EL units (**Fig. 1i**) by doping different elements such as copper and manganese into the ZnS phosphor[24]. Because the fibres are woven, the density of the EL units can be easily tuned by adjusting the weaving parameters to change the distances of the weft-warp contact points (**Fig. 1j**). The narrowest spacing we achieved here is approximately 800 μm.

To turn on the EL units, we applied alternating voltage to the luminescent warps and conductive wefts, generating a low microampere current to power the units (**Fig. 2a**). Electric-field-induced excitation of the luminescent centre and recombination of electron-hole pairs[25] result in light emission from the ZnS phosphor at the weft-warp contact area. By varying the applied electricity,

we could accurately tune the luminance of the EL unit. A luminance of 115.1 cd/m^2 was achieved at current density of 1.8 mA/cm^2 and power consumption of 363.1 μW (**Extended Data Fig. 3a-d**). At such a low power consumption, heating was negligible (**Extended Data Fig. 3e, f**), which is crucial for large-area clothing applications.

Because light emission also depends on how uniform the electric field is at the curved contact area between the luminescent warp and conductive weft, we used finite element method to simulate the electric field distribution in the luminescent layer (**Fig. 2b**). We found that the distribution at the curved contact under applied voltage was as uniform as a planar EL device (**Fig. 2b**, **Extended Data Fig. 4a-f**) and remained uniform even when the contact area was changed (**Fig. 2c**, **Extended Data Fig. 4g)**. We attribute this electric field homogeneity to the elastic conductive weft that readily deforms to fit the curved and less elastic surface of the luminescent warp (**Extended Data Fig. 1g, h**). Light emission occurred even when the conductive weft leaned, twisted and knotted with the luminescent warp (**Fig. 2d**, **Supplementary Movie 2**). EL mapping images show that EL intensities and unit areas remained nearly unchanged when the transparent conductive weft was moved along the luminescent warp (**Fig. 2e**), rotated around the contacting point (**Fig. 2f**), and bent with increasing bending angles (**Fig. 2g**). As the conductive weft slid along the luminescent warp at increments of 0.5 mm, the luminance varied by less than 2.2% for a distance up to 3 mm (**Fig. 2h**). When the transparent weft rotated by ±15° from the position perpendicular to the luminescent warp, the EL intensity fluctuated by less than 2.6% (**Fig. 2i**). Furthermore, due to the elasticity of the transparent weft, luminescence recovered instantly and remained stable over 100 cycles of pressing and releasing of the EL unit (**Fig. 2j**). Bending the transparent weft or luminescent warp up to 1.8 mm from its original state also resulted in fluctuations of less than 2.3% (**Fig. 2k, l**). Because the fibre is cylindrical, the EL intensity was well-maintained when the transparent weft was rolled around its central axis (**Extended Data Fig. 5**). The inert and non-volatile nature of the ionic liquid[26] in the transparent conductive weft also contributed to the electrical and optical stability of the EL unit (**Extended Data Fig. 6a, b**). Leaving the textile in the open air for 1 month did not show any obvious decrease in luminance (**Extended Data Fig. 6c**). When we coated the wefts and warps with a thin silicone protective layer, the brightness of the EL units endured repeated machine wash cycles (**Extended Data Fig. 6d-f**).

To show our weaving strategy is general, we used it to produce other electronic functions within

the textile (*e.g.*, keyboard and power supply). To create a textile keyboard that functions through dynamic contact, we wove low resistance warp (silver-plated yarn) with high resistance weft (carbon fibre) to form a 4×4 keyboard (**Extended Data Fig. 7a**), where the intersections of the weft and warp form the keypresses (**Extended Data Fig. 7b, c**). Pressing the keypress turns it on while releasing turns it off (**Extended Data Fig. 7d, e**). The keyboard works by reading the voltage between the metallic and carbon fibres (sample voltage, V_s) under an applied voltage (V_{cc}) of 5 V. Each keypress in the 4×4 keyboard is distinguished by the different sample voltage recorded when the keypress is pressed (**Extended Data Fig. 7f**). As power supply, we wove photoanode wefts with silver-plated conductive yarns to harvest solar energy (**Extended Data Fig. 8a-f**). The photoanode weft is a titanium (Ti) wire coated with a photoactive layer composed of titanium dioxide (TiO_2) nanotubes as the electron transport layer, dye molecules as sensitizer and copper iodide (CuI) as the solid electrolyte. Integrating these warps and wefts with battery fibres assembled from flexible MnO_2-coated carbon nanotube fibre (cathode), zinc wire (anode) and $ZnSO_4$ gel electrolyte, we realised both power generation and storage in the textile (**Extended Data Fig. 8g-i**). With display, keyboard and power supply, we can design a variety of multi-functional integrated textile systems for different applications (**Fig. 3a**, **Extended Data Fig. 9**).

As a proof-of-concept, we connected the woven display, keyboard and power supply to a display driver, microcontroller and Bluetooth module (**Fig. 3b**) and used the integrated textile system as an interactive navigation display (**Fig. 3c**). Through the Bluetooth module, real time location on a T-junction from a smartphone was transferred to the textile (**Fig. 3d).** To output the image on the display textile, electrical signals from the driver circuit are scanned row by row onto the array of EL units (**Fig. 3e**, **Supplementary Movie 3**). Our integrated textile system can also function as a communication tool, where information is input and displayed on the textile (**Fig. 3f**, **Supplementary Movie 3**). We demonstrate this using numbers '1', '2', and '3'. Each number is assigned a keypress and the microcontroller is programmed to output the number when the corresponding keypress is pushed (**Fig. 3g**). With the Bluetooth module, messages can also be sent, received and displayed between our integrated textile system and a smartphone (**Fig. 3h**).

To demonstrate the potential of display textiles in healthcare, we collected electroencephalogram signals from volunteers playing a race car game and those who were meditating. Brain waves in relaxed volunteers were mostly low frequency (**Fig. 3i**) while those in anxious volunteers were

158 mostly high frequency[27] (**Fig. 3j**). We processed the signals on a computer and sent words
159 corresponding to the mental state of the respective volunteers to the microcontroller through the
160 Bluetooth module for display. In the future, together with ways to decode complicated brain waves,
161 we envision display textiles like ours to become effective communication tools for individuals
162 with voice, speech or language disorders[28] (**Fig. 3k**). Such a tool will enable these individuals to
163 express themselves and reconnect with the world around them (**Fig. 3l**).
164
165 In summary, we present a functional, large-area display textile by weaving conductive and
166 luminescent fibres with cotton yarn to form EL units directly within the textile. Our method is
167 simple and can be used to weave other electronic functions such as a keyboard and power supply
168 into the textile to form a multi-functional integrated textile system for various applications.
169 Because of the network of wefts and warps, each EL unit in our display textile can be uniquely
170 identified and lit in a programmable way using a driver circuit. We show such an electronic textile
171 can be useful communication tools. With the integration of more functionalities, we expect these
172 smart textiles to form the communication tools of the future.
173

References

1. Larson, C. et al. Highly stretchable electroluminescent skin for optical signaling and tactile sensing. *Science* **351**, 1071–1074 (2016).
2. Tan, Y. J. et al. A transparent, self-healing and high-κ dielectric for low-field-emission stretchable optoelectronics. *Nat. Mater.* **19**, 182–188 (2020).
3. Tian, X. et al. Wireless body sensor networks based on metamaterial textiles. *Nat. Electron.* **2**, 243–251 (2019).
4. Chen, G. R., Li, Y. Z., Bick, M. & Chen, J. Smart textiles for electricity generation. *Chem. Rev.* **120**, 3668–3720 (2020).
5. Weng, W., Chen, P. N., He, S. S., Sun, X. M. & Peng, H. S. Smart electronic textiles. *Angew. Chem. Int. Ed.* **55**, 6140–6169 (2016).
6. Carey, T. et al. Fully inkjet-printed two-dimensional material field-effect heterojunctions for wearable and textile electronics. *Nat. Commun.* **8**, 1202 (2017).
7. Kim, J. et al. Ultrathin quantum dot display integrated with wearable electronics. *Adv. Mater.* **29**, 1700217 (2017).
8. Son, D. et al. An integrated self-healable electronic skin system fabricated via dynamic reconstruction of a nanostructured conducting network. *Nat. Nanotechnol.* **13**, 1057–1065 (2018).
9. Yin, D. et al. Efficient and mechanically robust stretchable organic light-emitting devices by a laser-programmable buckling process. *Nat. Commun.* **7**, 11573 (2016).
10. Rein, M. et al. Diode fibres for fabric-based optical communications. *Nature* **560**, 214–218 (2018).
11. Leber, A. et al. Soft and stretchable liquid metal transmission lines as distributed probes of multimodal deformations. *Nat. Electron.* **3**, 316–326 (2020).
12. Yang, A. N. et al. Fabric organic electrochemical transistors for biosensors. *Adv. Mater.* **30**, 1800051 (2018).
13. Hatamvand, M. et al. Recent advances in fiber-shaped and planar-shaped textile solar cells. *Nano Energy* **71**, 104609 (2020).
14. Jinno, H. et al. Stretchable and waterproof elastomer-coated organic photovoltaics for washable electronic textile applications. *Nat. Energy* **2**, 780–785 (2017).
15. Koo, J. H., Kim, D. C., Shim, H. J., Kim, T. H. & Kim, D. H. Flexible and stretchable smart display: materials, fabrication, device design, and system integration. *Adv. Funct. Mater.* **28**,

1801834 (2018).
16. de Mulatier, S., Nasreldin, M., Delattre, R., Ramuz, M. & Djenizian, T. Electronic circuits integration in textiles for data processing in wearable technologies. *Adv. Mater. Technol.* **3**, 1700320 (2018).
17. Wang, B. H. & Facchetti, A. Mechanically flexible conductors for stretchable and wearable e-skin and e-textile devices. *Adv. Mater.* **31**, 1901408 (2019).
18. Prieto-Ruiz, J. P. et al. Enhancing light emission in interface engineered spin-OLEDs through spin-polarized injection at high voltages. *Adv. Mater.* **31**, 1806817 (2019).
19. Fukagawa, H. et al. Long-lived flexible displays employing efficient and stable inverted organic light-emitting diodes. *Adv. Mater.* **30**, 1706768 (2018).
20. Conaghan, P. J. et al. Highly efficient blue organic light-emitting diodes based on carbene-metal-amides. *Nat. Commun.* **11**, 1758 (2020).
21. Zhou Y. et al. Bright stretchable electroluminescent devices based on silver nanowire electrodes and high-k thermoplastic elastomers. *ACS Appl. Mater. Interfaces* **10**, 44760−44767 (2018).
22. Li, S., Peele, B. N., Larson, C. M., Zhao, H. C. & Shepherd, R. F. A stretchable multicolor display and touch interface using photopatterning and transfer printing. *Adv. Mater.* **28**, 9770–9775 (2016).
23. Zhang, Z. T. et al. A stretchable and sensitive light-emitting fabric. *J. Mater. Chem. C* **5**, 4139–4144 (2017).
24. Yang, C. H., Chen, B. H., Zhou, J. X., Chen, Y. M. & Suo, Z. G. Electroluminescence of giant stretchability. *Adv. Mater.* **28**, 4480–4484 (2016).
25. Chen, F. & Xiang, Y. *AC Powder Electroluminescence in Luminescent Materials and Applications* (John Wiley & Sons, Chichester, 2008).
26. Jin, M. L. et al. An ultrastable ionic chemiresistor skin with an intrinsically stretchable polymer electrolyte. *Adv. Mater.* **30**, 1706851 (2018).
27. Müller-Putz, G. R., Riedl, R. & Wriessnegger, S. C. Electroencephalography (EEG) as a research tool in the information systems discipline: foundations, measurement, and applications. *Commun. Assoc. Inf. Syst.* **37**, 912–948 (2015).
28. Voice, speech and language research, https://www.nidcd.nih.gov/about/strategic-plan/2017-2021/voice-speech-and-language-research (2017).

Methods

Preparation of the transparent conductive weft

Polyurethane ionic gel fibre was spun from the transparent ionic-liquid-doped polyurethane gel. Thermoplastic polyurethane (TPU) (Covestro, Desmopan® 2786A) was firstly dissolved in N, N-dimethylformamide (DMF) (Sinopharm) with a weight ratio of 1/4 under mechanically stirring at 80 °C for 2 h. Subsequently, 1-ethyl-3-methylimidazolium:bis (trifluoromethylsulfoyl) imide ($[EMIM]^+[TFSI]^-$) ionic liquid (Aladdin) was added to the above TPU-DMF solution for further stirring (80 °C for 1 h). The ionic gel flake was obtained by totally removing the solvent of DMF in an oven box at 80 °C for 12 h. Then melt-spinning was carried out using 3D printing system (3D Bio-Architect® work station, Regenovo) with 0.25 mm inner diameter nozzle. The transparent conductive weft was extruded at a melting zone temperature of 180 ℃ and cooled at room temperature. To achieve water resistance, silicone protective layer (Dow Corning, 1-2577) could be further dip-coated on the transparent conductive wefts.

Preparation of the luminescent warp

Commercially available ZnS phosphors (Shanghai Keyan Phosphor Technology Co., Ltd.) were dispersed in waterborne polyurethane (U-9, Shanghai Sisheng Polymer Materials Co., Ltd.) with a weight ratio of 3/1 by mechanical stirring for 20 min. After degassing in a vacuum oven, the as-prepared mixtures were loaded on the silver-plated nylon yarns (100D, Hengtong X-silver Speciality Textile Co., Ltd.) on a continuous producing line. Silver-plated yarns were dipped into the ZnS phosphor dispersions and passed through the centre of a scraper ring in inner diameter of 0.32 mm, followed by drying under 120 °C in a 2-metre-long air-dry oven. The moving speed of yarns was 10 m/min. Coating process was conducted for three times to prepare luminescent warp in diameter of ~0.3 mm. To achieve water resistance, silicone protective layer (Dow Corning, 1-2577) could be further dip-coated on the luminescent warps.

Fabrication of the display textile

The weaving operation of the display textile was made on a rapier loom (Tong Yuan Textile Machinery Co., Ltd.). The weave diagram was presented in **Fig. 1a**. Note that other fibre materials

such as polyurethane-coated metal wire can be also co-woven inside.

Structure and performance characterization of EL units

The cross-sectional image of the single EL unit was obtained from scanning electron microscopy (S-4800, Hitachi) operated at 1 kV. The transparency of the ionic gel was characterized by an UV-visible spectrophotometer (UV-2550 SHIMADZU Spectrometer) to scan wavelengths from 450 to 700 nm. The luminance of a single EL unit was detected by a spectrophotometer (Photoresearch PR-680) under an alternating voltage supplied by a function waveform generator (Keysight 33500B Series) connected with a high-voltage power amplifier (610 E, TREK Inc.). If not specified, the test parameters of the EL unit were 1.2 V/μm and 2 kHz, and the intersection area in EL unit projection was used as effective device area. The voltage, current and power consumption were measured (Keysight 34461A Digit multimeter) using a test circuit (see **Extended Data Fig. 3d** for details). The EL mappings of EL units under bending, sliding and rotating were obtained by mapping the photographs according to the gray value in Matlab. For statistical analysis of relative EL intensity of the units in the display textile, the gray values of the units were extracted from the photographs by ImageJ, which had been captured by a digital camera (D3400, NIKON) in dark room. Uniformity of EL unit array was evaluated according to relative deviation (RD) calculated by $RD=(L_x-\overline{L})/\overline{L}\times 100\%$, where L_x was the EL intensity of a single EL unit, and $\overline{L}$ was the average intensity of 600 units. Stability of EL unit array was evaluated by counting the EL intensity variation (calculated as L/L_0, where L_0 and L were the intensities before and after deforming, respectively) of 600 EL units. The temperature changes of EL units were measured by an infrared camera (PI 640, Optris).

Washing test of display textile

The washing tests were conducted in a standard washing machine (SW-12E, Nantong Hongda Experimental Instrument Co., Ltd.) (**Extended Data Fig. 6d**). Each EL unit was woven into a 2×2 cm textile and put into individual washing chamber containing 200 g water and 0.8 g detergent. After washed for 30 min in room temperature, the textiles were rinsed under flowing water and dried under 60 °C for 1 h. The test parameters of EL performance were 3 V/μm and 2 kHz.

Calculation of power consumption of an EL unit

The voltage at the certain position (the root mean square at A, B, C, Ground, referred to **Extended Data Fig. 3d**) and the resistance of each resistor were firstly measured. The current across each resistor was calculated as $I = V/R$. The current through Resistors 2 and 3 was:

$$I_2 = \frac{V_{AB}}{R_2} = I_3 \qquad (1)$$

Using Equation 1, V_{AC} was calculated (the voltage across the entire test circuit):

$$V_{AC} = V_{AB} + V_{BC} = I_2 R_2 + I_3 R_3 \qquad (2)$$

The current across R_1 was equal to the total current through the test circuit. Based on this equality, the power of the test circuit was:

$$P_{total} = I_1 V_{AC} \cos\theta \qquad (3)$$

where θ represented the phase shift between the current and voltage waveforms across the test circuit. This phase shift was measured using an oscilloscope (TDS 2012C, Tektronix). Hence, the real power of the test circuit, which included energy used by the EL unit and the resistors, could be calculated according to:

$$P_{total} = P_{unit} + P_{resistor} \qquad (4)$$

The power consumption of the EL unit was obtained by subtracting the power consumption of the resistor. The power consumed by each resistor was calculated by the equation of $P = I^2R$.

Electric-field simulation of the EL unit through finite element method

The EL unit was constructed in ABAQUS CAE with geometry characteristics in **Extended Data Fig. 1i**. 8-node linear reduced-integration hybrid brick elements (C3D8RH) were used to model the transparent conductive weft of hyperelastic materials. Through mesh convergence study, 30284 and 39840 elements were generated for the luminescent warp and the transparent conductive weft, respectively.

Mechanical properties of materials were defined by directly importing the uniaxial tensile test data (**Extended Data Fig. 1**). Linear elastic model was employed for luminescent warp. Ogden

hyperelastic model was employed for the polyurethane ionic gel fibre with the strain energy potential function W:

$$W = \frac{2\mu_1}{\alpha_1^2}\left(\bar{\lambda}_1^{\alpha_1} + \bar{\lambda}_2^{\alpha_1} + \bar{\lambda}_3^{\alpha_1} - 3\right) + \frac{1}{D_1}(J-1)^2$$

Where $\bar{\lambda}_i$ is the deviatoric principal stretches $\bar{\lambda}_i = J^{-\frac{1}{3}}\lambda_i$. Here λ_i is the principal stretches. This form could be degenerated into Neo-Hookean form of potential energy when $\alpha_1 = 2$.

As mentioned above, periodic boundary conditions were imposed along the axial direction of the transparent conductive weft. The axial length of EL unit was fixed since the weft was kept tight during weaving process. Contact between transparent conductive weft and luminescent warp was defined as default hard contact. The loads imposed on both ends of the transparent conductive weft were estimated by outputting the reaction force of the polyurethane ionic gel fibre under a displacement of 0.48 mm.

Static electric analyses were then conducted on the deformed models to obtain the electric fields in the ZnS phosphor layer. The transparent conductive weft was grounded and 90 V electric potential was imposed on the core conductive yarn of luminescent warp. The dielectric constant of the luminescent layer was 3.621×10^{-11} F/m.

Fabrication of textile keyboard

The textile keyboard was based on a jacquard method by weaving carbon fibres (1K, TORAY, Japan), silver-plated yarns and cotton yarns according to the weave diagram in **Extended Data Fig. 7a**.

Fabrication of energy harvesting and storing textile

Ti wire (diameter of 127 μm, Alfa Aesar) was used as the substrate of photoanode. First, the Ti wire was sequentially cleaned by sonication in deionized water, acetone and isopropanol for 5 min each. Then TiO_2 nanotubes were grown on Ti wire by an anodic oxidation in a water bath. A 0.3 wt% NH_4F/ethylene glycol (Sinopharm) solution containing 8 wt% H_2O was prepared as the electrolyte. The growth was operated in a two-electrode system with Ti wire as anode and Pt plate as cathode at 60 V for 2 h. The modified Ti wire was washed and annealed at 500 °C for 60 min.

After cooled to 110 °C in the furnace, the wire was immersed in Z907 (Shanghai MaterWin New Materials Co., Ltd.) solution (0.3 mM, mixture solvent of dehydrated acetonitrile (Adamas) and tert-butanol (Sinopharm) with an equal volume ratio) for 16 h. Next, CuI was drop-coated onto the modified Ti wire in a glovebox at 110 °C. CuI solution was prepared by dissolving 0.16 M cuprous iodide (Aladdin), 1-methyl-3-ethylimidazolium thiocyanate (Lanzhou Greenchem ILs) and 0.2 mM 4-tert-butylpyridine (Adamas) in acetonitrile.

The aqueous zinc ion battery fibre was composed of a MnO_2 coated carbon nanotube (CNT) fibre cathode, a zinc wire anode, and gelation/$ZnSO_4$ water-based gel electrolyte[29]. A CNT fibre was first synthesized by floating-catalyst method[30]. For the fibre cathode, MnO_2 was electrodeposited onto the CNT fibre through a scalable electrodeposition method (pulse mode 1.5 V for 1 s and 0.7 V for 10 s) in electrolyte containing 0.1 M $Mn(Ac)_2•4H_2O$ (Aladdin) and 0.1 M Na_2SO_4 (Sinopharm) with an Ag/AgCl reference electrode and a Pt counter electrode. The MnO_2 loading mass was 0.5 mg/cm for the cathode fibre. The zinc wire with a diameter of ~0.5 mm was polished and rinsed before use. The cathode and anode wires were uniformly coated with gel electrolyte and then twisted together. The gel electrolyte was prepared by firstly dissolving 1.0 g gelatin (Sinopharm) and 0.1 g $Na_2B_4O_7$ (Aladdin) in 10 mL deionized water at 80 °C. Then 10 mM $ZnSO_4•7H_2O$ (Aladdin) and 1 mM $MnSO_4•H_2O$ (Aladdin) were added under stirring until a homogenous solution was formed. The as-fabricated battery was dried at room temperature, and the gel electrolyte concurrently served as electrolyte and separator. The battery was put into a flexible poly (vinyl chloride) tube and sealed by resin adhesive at the terminals of the tube.

Silver-plated nylon yarns were woven in the warp direction as the counter electrodes for energy harvesting part and the electrical connections for energy storing part. The cotton threads, modified photoanode fibres and zinc-ion battery fibres were then alternately woven in the weft direction. Current density-voltage curves of the energy harvesting part were recorded by a Keithley 2400 Source Meter under the illumination (100 mW/cm^2) of simulated AM1.5 solar light from a solar simulator (Oriel-Sol3A 94023A equipped with a 450 W Xe lamp and an AM1.5 filter). Electrochemical measurements were performed on an electrochemical workstation (CHI 660a).

Fabrication of the integrated textile system

Different electronic textiles were arranged on a piece of cloth by changing functional fibres during weaving process, which were integrated on a jacket by hot melt adhesive or sewing. The microcontroller of textile electronics was STM32F103T8U6, an ARM32-bit CortexTM-M3 CPU with QFN36 package (DM14580). By using an analog-to-digital converter to sample the keyboard resistance, the single bus detection of the keyboard was realised. Driving circuit of display textile was provided by Shanghai Mi Fang Electronics Co., Ltd. The communication between integrated textile system and mobile phone was realised by Bluetooth module (HC-05). If necessary, the other commercial portable power source could be also integrated as backup power.

Collection and decoding of electroencephalogram signals

The signals of volunteers were collected by the wearable recorder (MindWave Mobile 2, Neurosky). The volunteers were asked to play a car race game to be in an anxious mental state and lay back in meditation to be in a relaxed mental state. The signals were recorded in real time and collected on a computer. After downsampled to 100 Hz, the signals were filtered by 4th-order IIR bandpass filters with bandwidth of 0.1–48 Hz. The time domain signals were transferred to spectrogram by fast Fourier transform.

Data availability

All data are contained within the manuscript. Raw data are available from the corresponding authors upon reasonable request.

Code availability

Custom code used in this study is available from the corresponding authors upon reasonable request.

29. Wang, Z. F. et al. A flexible rechargeable zinc-ion wire-shaped battery with shape memory function. *J. Mater. Chem. A* **6**, 8549–8557 (2018).
30. Lee, J. et al. Direct spinning and densification method for high-performance carbon nanotube fibers. *Nat. Commun.* **10**, 2962 (2019).

Acknowledgements

This work was supported by MOST (2016YFA0203302), NSFC (21634003, 51673043, 21805044, 21875042), STCSM (18QA1400800, 19QA1400800), SHMEC (2017-01-07-00-07-E00062), and Yanchang Petroleum Group. Part of the sample fabrication was performed at Fudan Nano-fabrication Laboratory. We thank Shanghai Mi Fang Electronics Co., Ltd. for technical support of the display driving circuits, Idea Optics Co., Ltd. for offering test instruments, Jiaying Zhao for assistance in textile weaving, and Ai Lin Chun of Science Storylab for critically reading and editing the manuscript.

Author contributions

H. P. and P. C. conceived and designed the research project. X. Shi. and Y. Z. and P. Z. performed the experiments on the display textile, keyboard and integration systems and contributed equally to this work. J. S. and Y. Y. and Q. T. performed the simulation. Z. G. performed the experiments on photovoltaic textiles. M. L. and J. W. performed the experiments on energy storage fibres. X. Shi. and Y. Z. and P. Z. and X. X. analysed the data. B. Z., X. Sun., L. Z., Q. P., D. J. and all other authors discussed the data and wrote the paper.

Competing interests

The authors declare no competing interests.

Additional information

Supplementary Information is available for this paper.

Correspondence and requests for materials should be addressed to P. C. (peiningc@fudan.edu.cn) and H. P. (penghs@fudan.edu.cn).

Figures

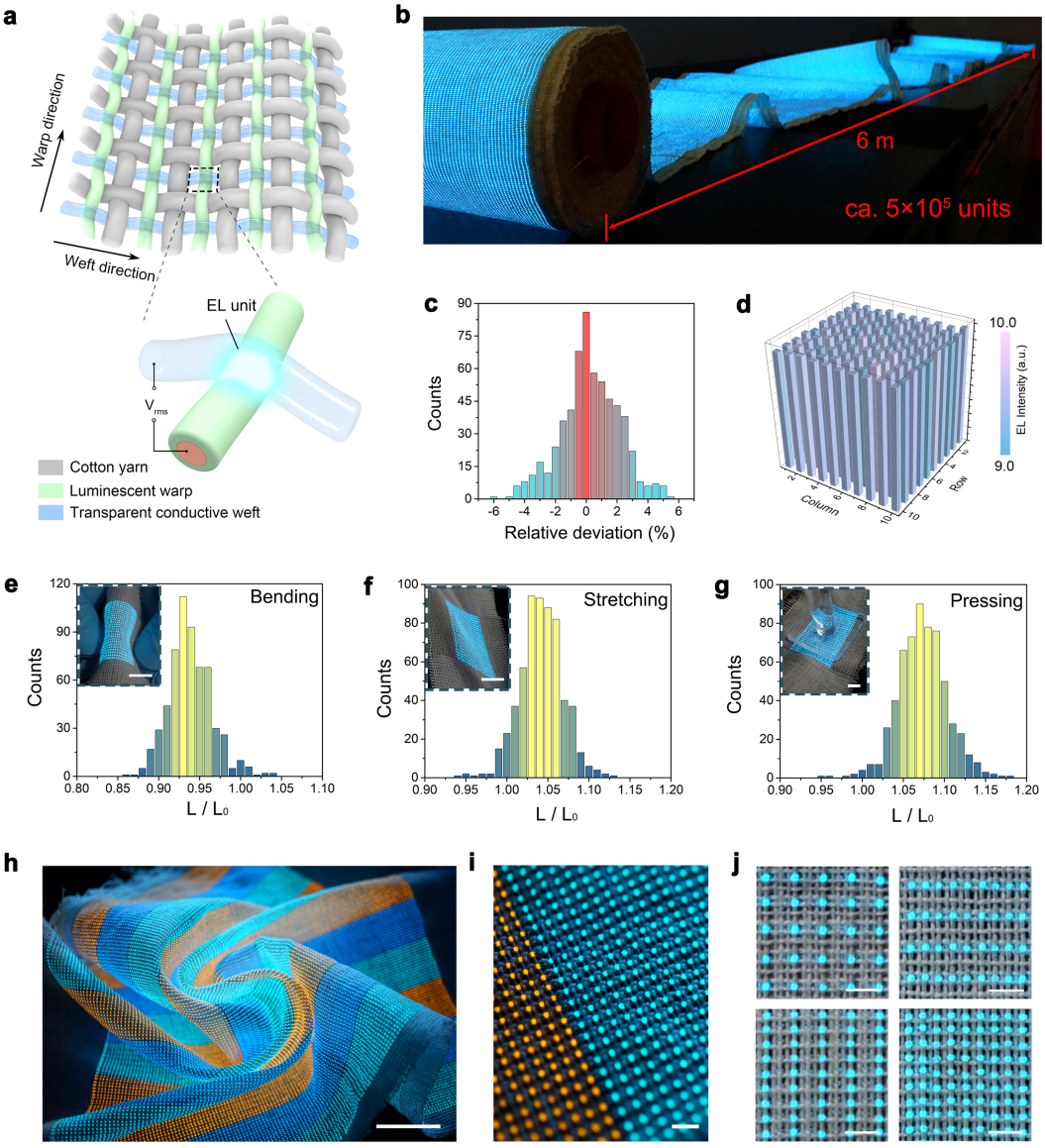

Fig. 1 | Structure and EL performance of the display textile. a, Schematic showing the weave diagram of the display textile. Each contacting luminescent warp and transparent conductive weft forms an EL unit (inset). Applied alternating voltage (V_{rms}) turns on the EL units. **b**, Photograph of a 6-metre-long display textile consisting of approximately 5×10^5 EL units. **c**, Statistical distribution shows the relative deviations of emission intensity for 600 EL units examined are between -6.3% and 5.2%. Relative deviation is defined as deviation of luminance for a single EL unit from the average value. **d**, Emission intensities of a 10×10 EL unit array is uniform (< 10%

differences in intensity among the units). **e-g**, Statistical distribution shows minor (< 10%) variations in luminance for 600 EL units after 1,000 cycles of bending (**e**), stretching (**f**), and pressing (**g**). Insets: photographs of tested samples. Scale bars, 1 cm. **h**, Photograph of a functional multicolour display textile under complex deformations, including bending and twisting. Blue and orange are achieved by doping ZnS with copper and manganese, respectively. Scale bar, 2 cm. **i**, Magnified photograph of the multicolour display textile from **h** show EL units are uniformly spaced at a distance of ~800 μm. Scale bar, 2 mm. **j**, Photographs of EL units spaced at different distances obtained by changing the weaving parameters. Scale bars, 2 mm.

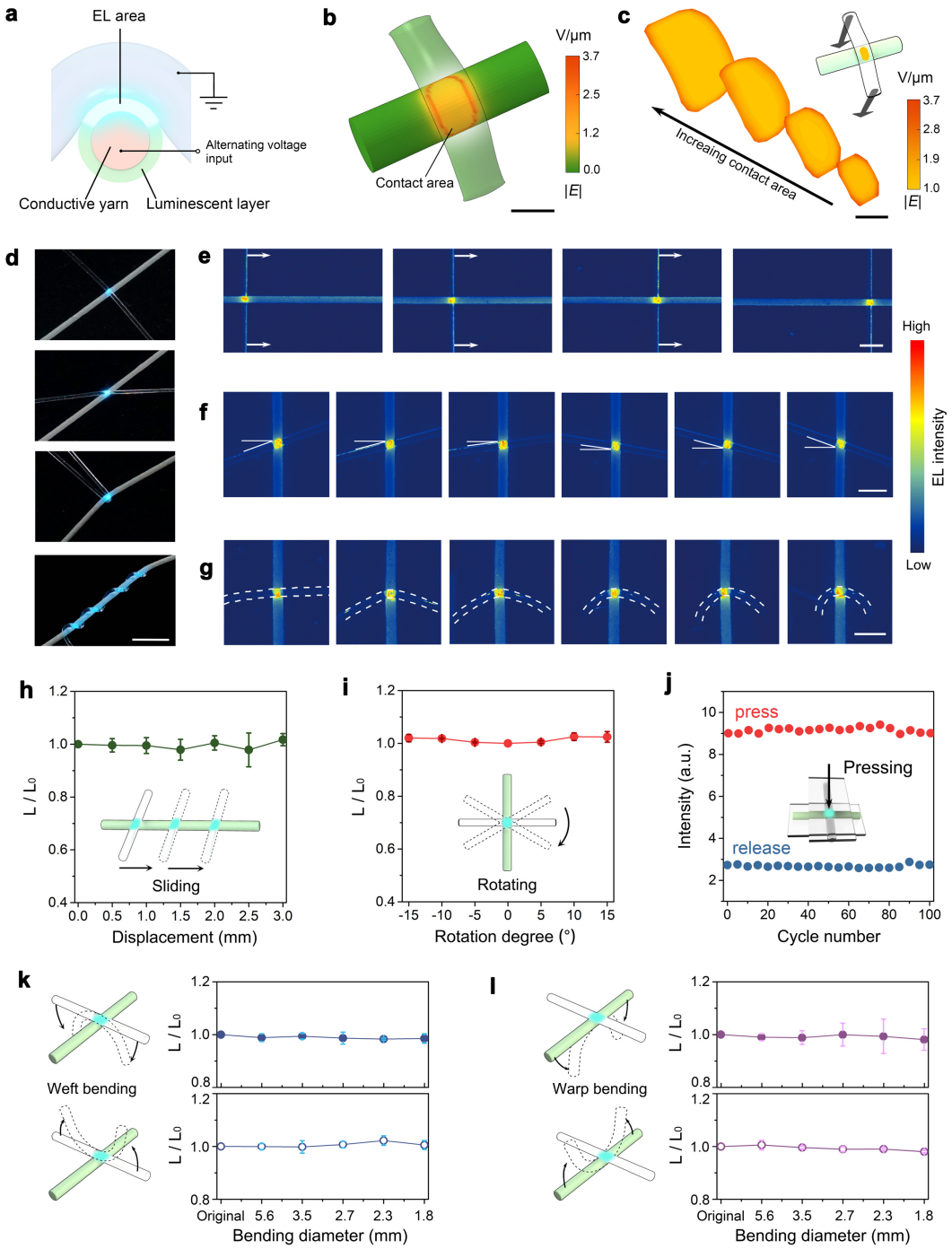

Fig. 2 | Characterization of EL units of the display textile. a, Schematic of an EL unit formed at the contact area between luminescent warp and transparent conductive weft. Light emission occurs when an alternating electric voltage is applied. **b**, **c**, Simulation using finite element method shows electric field distribution at the contact area in an EL unit is uniform (**b**) and does not change

with increasing contact areas (**c**). **d**, Photographs show stable light emission as the transparent conductive weft contacted, leaned, twisted and knotted with the luminescent warp (top to bottom). Scale bar, 2 mm. **e-g**, EL maps show brightness of EL units remained stable even when the transparent weft is slid (**e**), rotated (**f**) and bent (**g**) along the luminescent warp. Colour bar indicates relative EL intensity. Scale bars, 1 mm. **h**-**l**, Luminance varied minimally when the transparent weft is moved by 3 mm along the luminescent warp (**h**) and rotated by different degrees (**i**; 0° is when the weft is perpendicular to the warp), and when the EL unit is pressed and released for 100 cycles (**j**), bent along the weft length (**k**) and along the warp length (**l)** with increasing bending angles. L_0 and L correspond to the EL intensity before and after deformation, respectively. Error bars are standard deviations of the results from at least three samples.

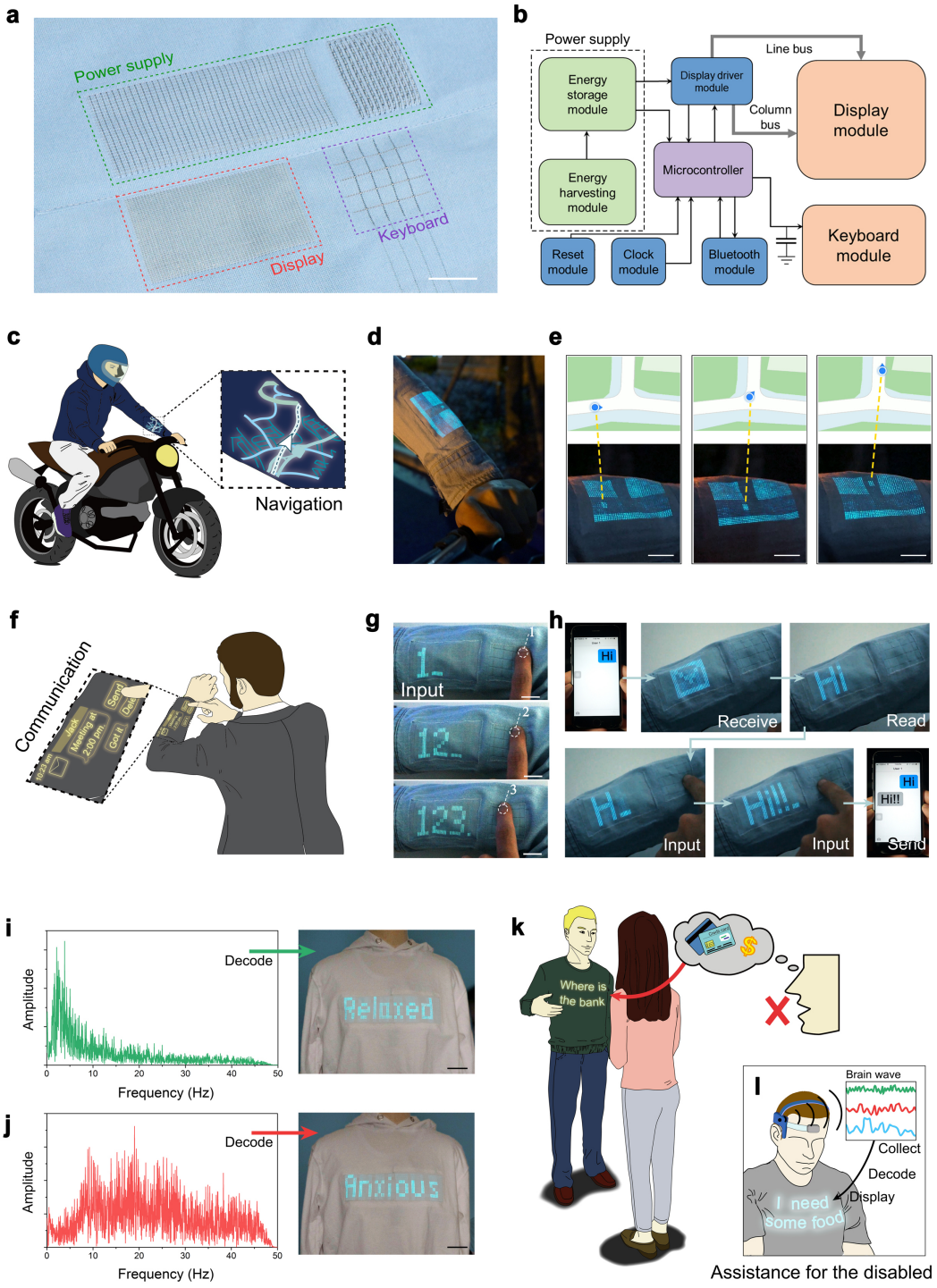

Fig. 3 | Application scenarios of integrated textile systems. a, Photograph of an integrated textile system consisting of display, information input (keyboard) and power supply modules. Scale bar, 2 cm. **b**, System-level block diagram of the integrated textile system in **a** shows the modules

connected to a microcontroller that is powered by solar energy harvesting and electrical energy storing modules. **c**, Schematic illustrating the integrated textile as a smart node for the Internet of Things to offer location services during driving. Selective illumination on the display module is achieved by scanning electrical signals from the driver circuit row by row onto the array of EL units. **d**, **e**, Real-time location at a T-junction on a sleeve, transferred through the Bluetooth and microcontroller modules, is synchronized with the location map on a smartphone. Scale bars, 1 cm. **f**, Schematic shows textiles integrated with a display and keyboard can be used as a communication platform. **g**, Information is input onto clothes by pressing the keypress that is woven into the textile. Scale bars, 2 cm. **h**, Receiving and sending messages between the integrated textile system and a smartphone. **i**, **j**, Expressions of mental states by decoding representative electroencephalogram signals. The words "Relaxed" (**i**) and "Anxious" (**j**) are displayed on clothes when the dominant brain waves are detected in the low-frequency region (0–10 Hz) and high-frequency region (10–40 Hz), respectively. Scale bars, 5 cm. **k**, Display textiles could in the future enable individuals with speech disorders to communicate and express themselves. **l**, Conceptual image showing brain waves from a disabled person are being decoded into messages that are displayed on a shirt made from an integrated textile.

Extended Data Figures

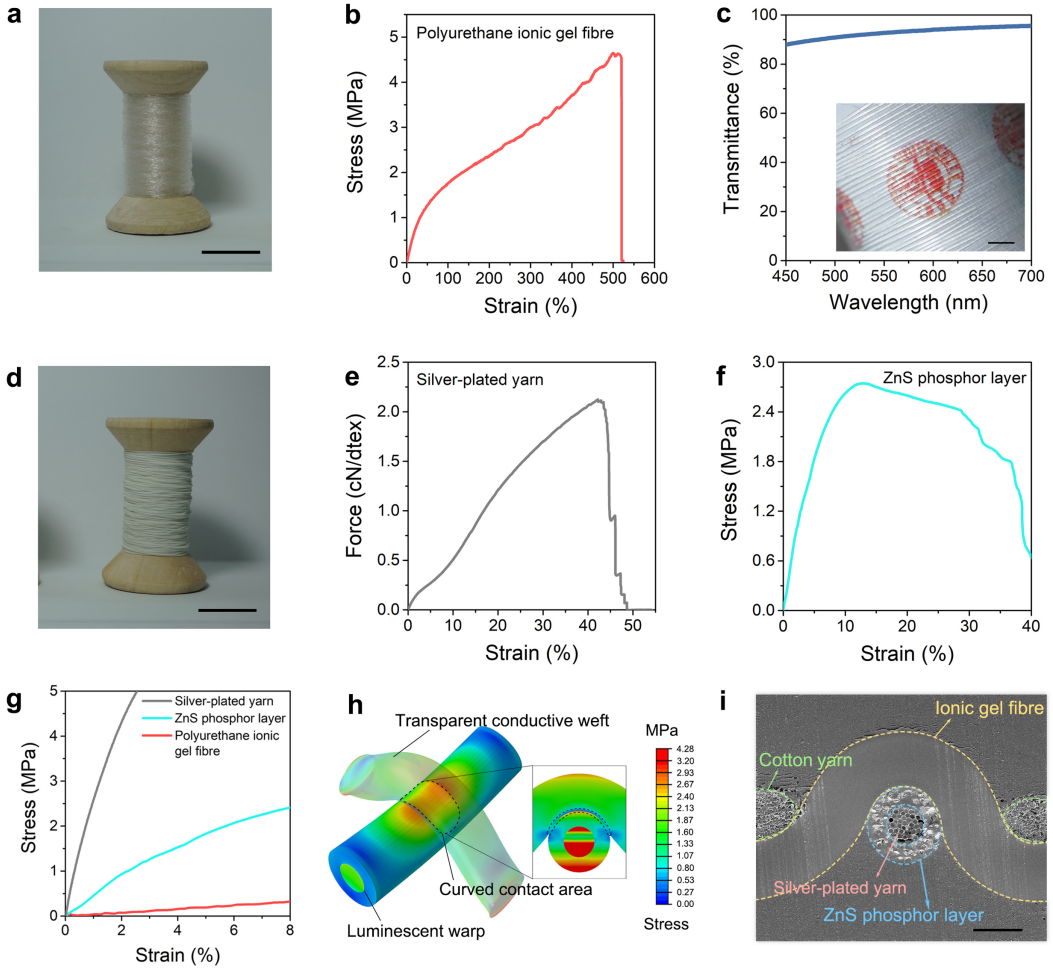

Extended Data Fig. 1 | Mechanical characterization of transparent conductive weft, luminescent warp and their contact area. a, Photograph of transparent conductive wefts on a spool. Scale bar, 2 cm. **b**, Stress-strain curve of polyurethane ionic gel fibre. **c**, Transmittance of ionic gel film with thickness of 250 μm. The inset is transparent conductive weft wound on a spool. Scale bar, 2 mm. **d**, Photograph of luminescent warps on a spool. Scale bar, 2 cm. **e**, Force-strain curve of silver-plated yarn. **f**, Stress-strain curve of ZnS phosphor layer. **g**, Comparison of mechanical properties of silver-plated yarn, ZnS phosphor layer and polyurethane ionic gel fibre. **h**, Deformation and stress simulation in an EL unit. **i**, Cross-sectional SEM image of an EL unit after embedded in resin. Scale bar, 200 μm.

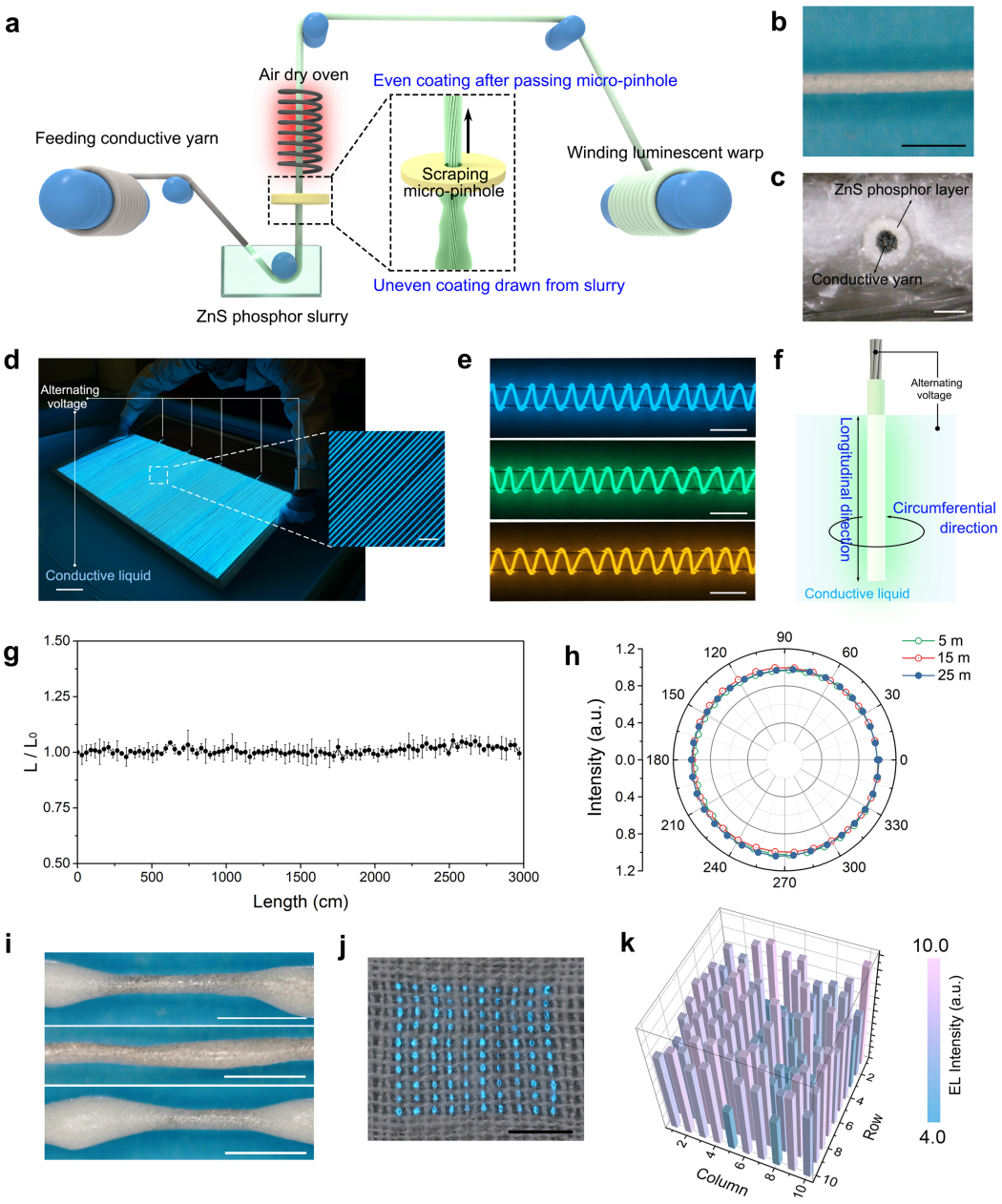

Extended Data Fig. 2 | Longitudinally and circumferentially homogeneity of luminescent warp. a, Schematic illustration of continuous fabrication of luminescent warp. **b**, Optical image of luminescent warp. Scale bar, 1 mm. **c**, Cross-sectional image of luminescent warp. Scale bar, 200 μm. **d**, Photographs for ~100-metre-long luminescent warp parallelly arranged on a board in a salt water pool. Scale bar, 10 cm. The luminescent warp is lightened by applying alternating voltage upon luminescent warp and salt water. The magnified area indicates the homogeneous

luminescence along the fibre. Scale bar, 5 mm. **e**, Multicolour luminescent warps wound on a glass stick and lightened in salt water. Scale bars, 5 mm. **f**, Schematic of longitudinal and circumferential direction of luminescent warp. **g**, Luminance distribution along the length of luminescent warp. Error bars represent the standard deviations of the results from three samples. **h**, Luminance distribution around the luminescent warp circumference. **i**, Uneven luminescent layer in the case that without using scraping micro-pinhole. Scale bars, 1 mm. **j**, Photograph of the display textile woven from luminescent warps with uneven coating. Scale bar, 5 mm. **k**, Relative emission intensities of a 10×10 EL unit array in **j**.

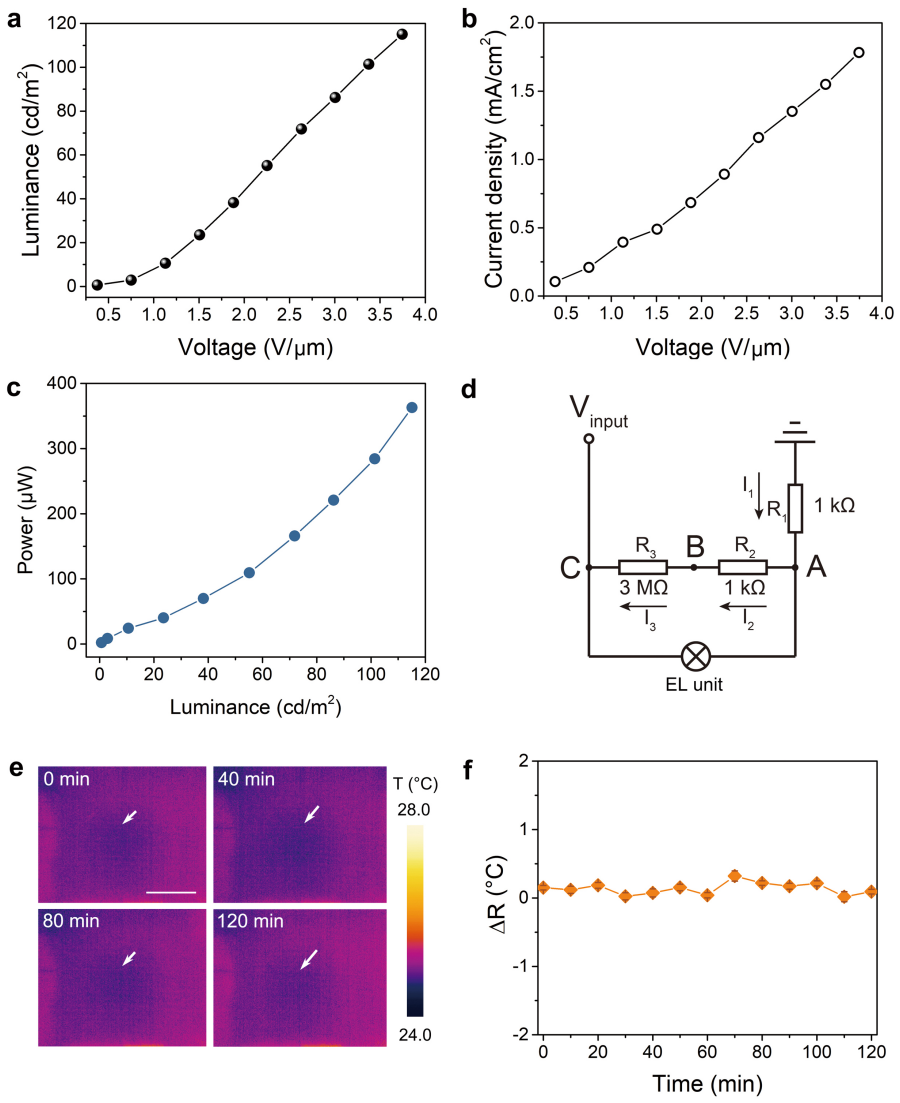

518

519

520 **Extended Data Fig. 3 | EL performance of the EL unit. a-c**, Luminance-voltage (**a**), current
521 density-voltage (**b**), and power-luminance (**c**) characteristics of the EL unit. **d**, Test circuit for
522 measuring power consumption of the EL unit. **e**, Thermal images of an illuminating EL unit along
523 increasing durations (under a power of ~300 μW). The arrows indicate the position of the EL unit.
524 Scale bar, 5 mm. **f**, Local temperature variations of EL units under a power of ~300 μW. Error bars
525 represent the standard deviations of the results from five samples.

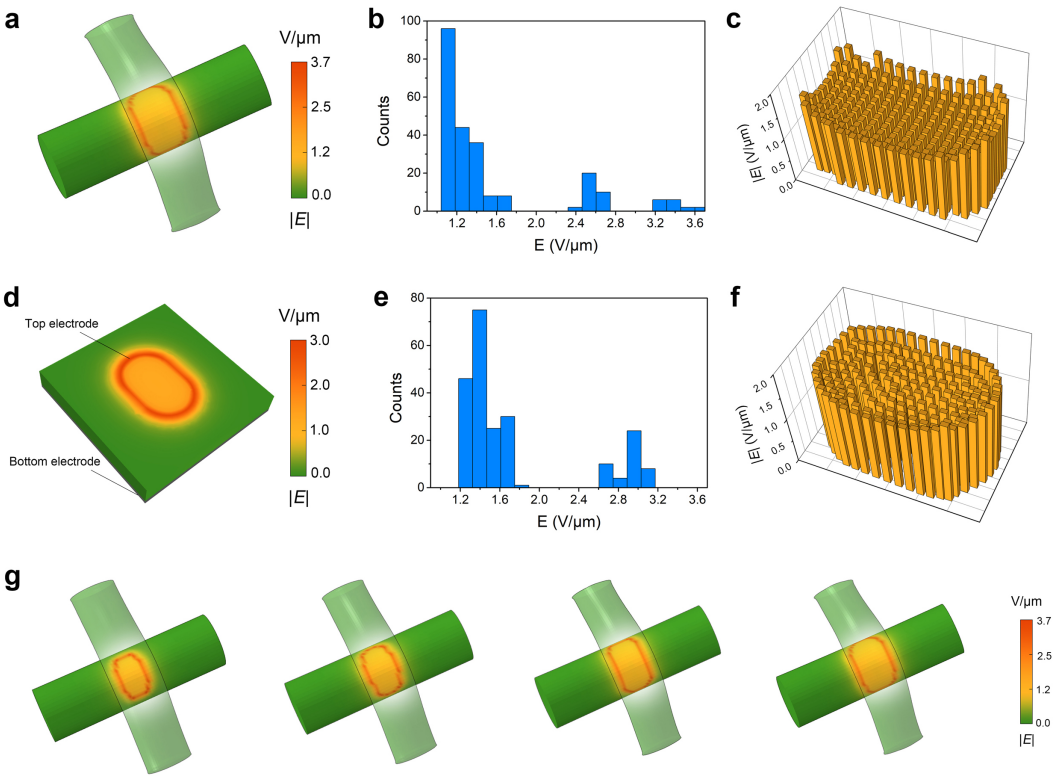

526

527

528 **Extended Data Fig. 4 | Comparison of electric field distribution of curved and planar contact**
529 **areas.** Electric field distribution in woven EL unit (**a-c**) and traditional planar sandwiched EL
530 devices (**d-f**). **a**, **d**, Electric field distribution, **b**, **e**, statistics of the simulation elements on contact
531 area according to the electric field values, and **c**, **f**, visualization of electric field values by the
532 height of bars. **g**, Electric field distributions of EL unit along with increasing contact areas.

533

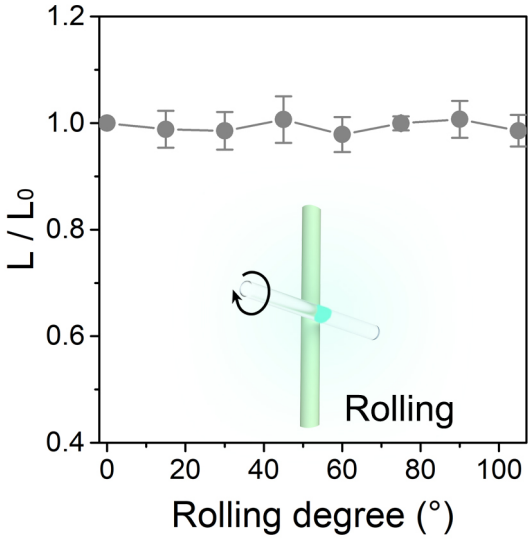

Extended Data Fig. 5 | Luminance variations when the transparent conductive weft is rolled around its central axis. Error bars represent the standard deviations of the results from three samples. L_0 and L correspond to the EL intensity before and after deformation, respectively.

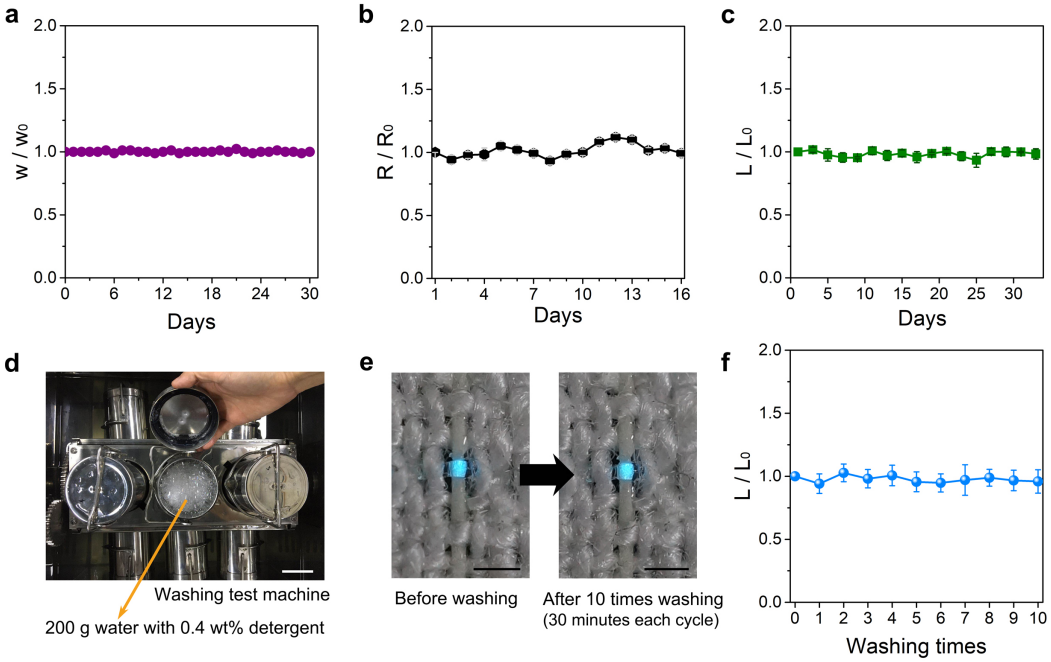

Extended Data Fig. 6 | Durability of polyurethane ionic gel fibre and EL units. a, **b**, Variation of weight (**a**) and electrical resistance (**b**) for the polyurethane ionic gel fibre in open air at room temperature. Here w_0 and w correspond to the weights before and after exposure to the air, respectively; R_0 and R correspond to the electrical resistances before and after exposure to the air, respectively. **c**, EL performance of EL units stored in open air. L_0 and L correspond to the EL intensity before and after exposure to the air, respectively. **d**, Photograph of inner structure of washing machine. Scale bar, 5 cm **e**, Luminescence of EL unit before and after 10 cycles of machine wash (30 minutes each cycle). Scale bar, 500 μm. **f**, Luminance variations when EL units were washed and dried for 10 cycles. L_0 and L correspond to the EL intensity before and after washing, respectively. Error bars represent the standard deviations of the results from at least three samples.

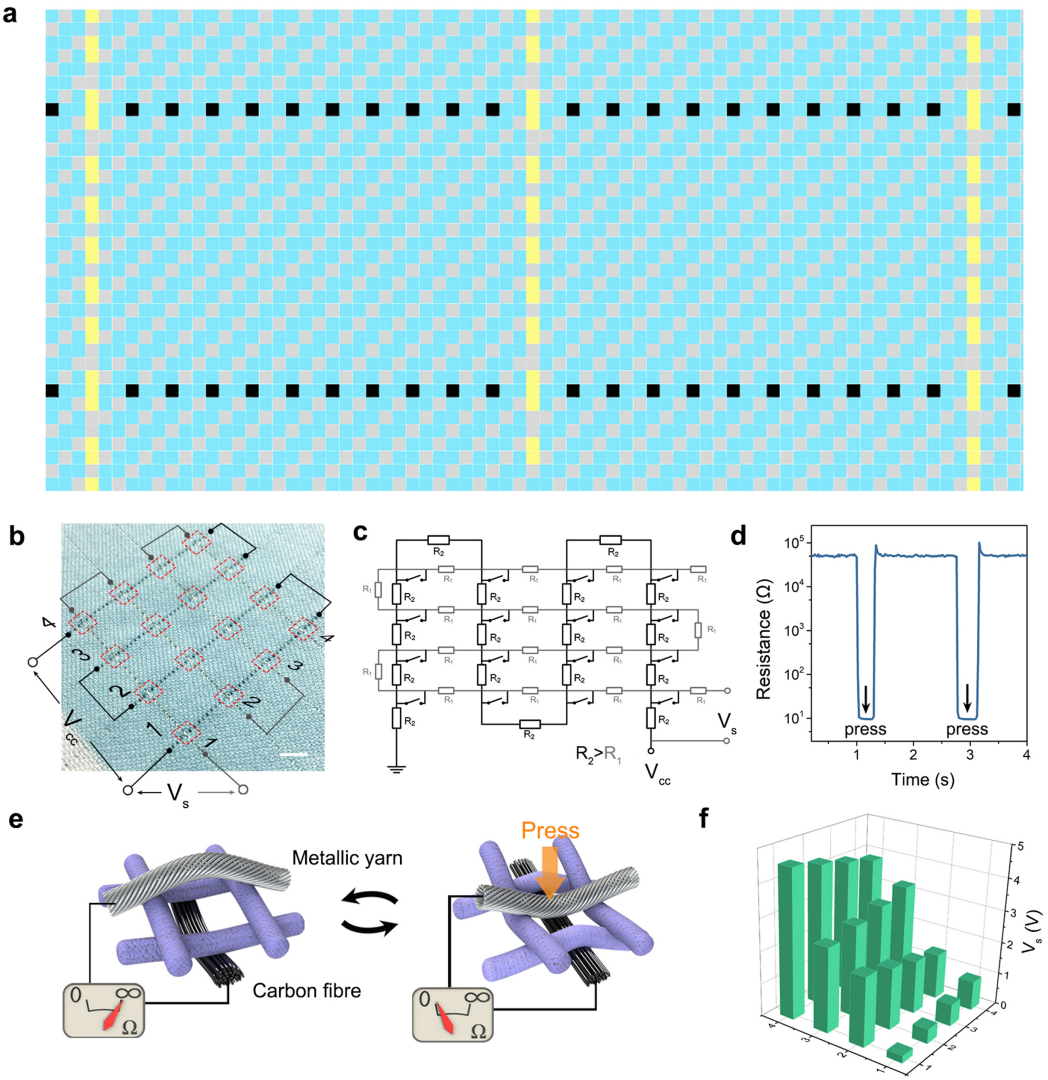

Extended Data Fig. 7 | Characterization of textile keyboard. a, Weave diagram of the textile keyboard (yellow: Ag-plated fibre, black: carbon fibre, blue: cotton yarn, gray: cotton yarn). **b**, Photograph and electrical connection of a 4×4 textile keyboard. The red squares indicate the positions of keypresses. Scale bar, 5 mm. **c**, Equivalent circuit of a 4×4 keyboard. This keyboard worked by reading the voltage between the metallic and carbon fibres (sample voltage, V_s) at an applied voltage (V_{cc}) of 5 V. **d**, Pressing responses of a keypress with resistance variations that were greater than 4 orders of magnitude. **e**, Working mechanism of the textile keyboard. **f**, Voltages (V_s) recorded by pressing individual keypresses one by one. The correspondence between the keypress position and its characteristic V_s are indicated by the coordinates in **b** and **f**.

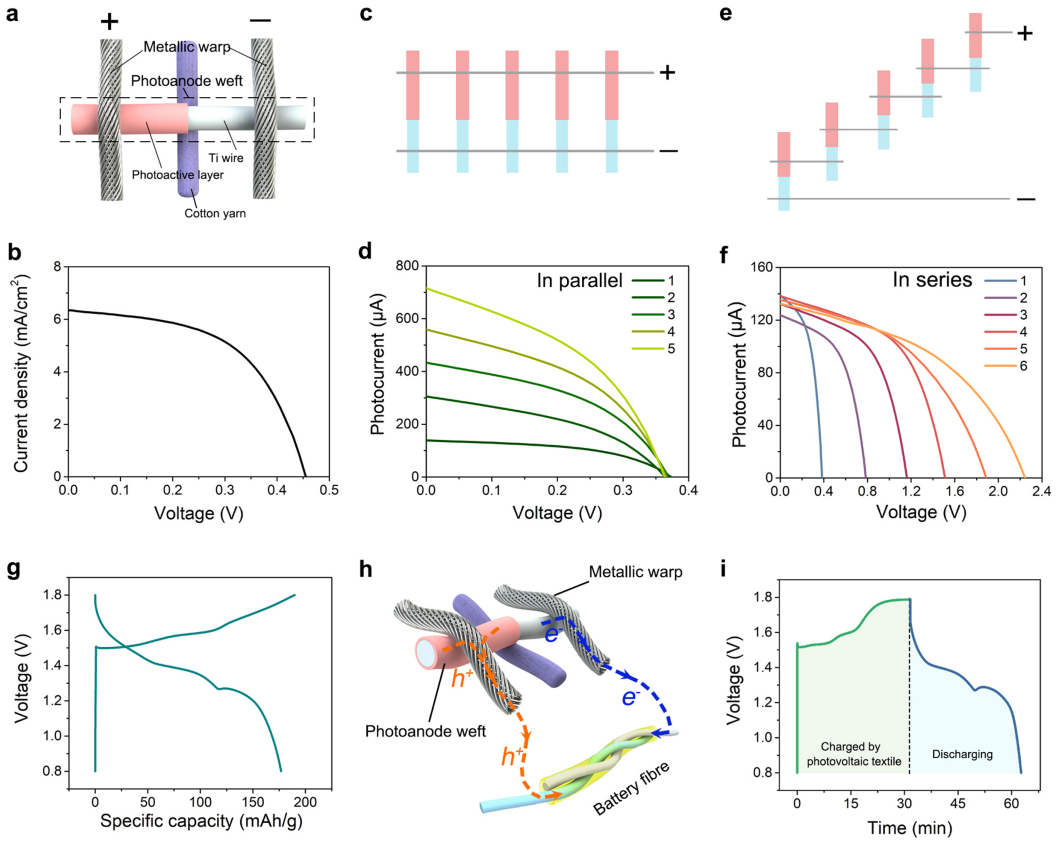

Extended Data Fig. 8 | Characterization of textile power supply system. a, Schematic of a woven photovoltaic unit. **b**, Current density-voltage characteristics of the photovoltaic unit, exhibiting a short-circuit current density of 6.32 mA/cm^2 and an open-circuit voltage of 0.45 V. **c**, Schematic of the woven photovoltaic units connected in parallel. **d**, Current-voltage curve of the photovoltaic textile with increasing numbers of photoanode wefts connected in parallel. **e**, Schematic of the woven photovoltaic units connected in series. **f**, Current-voltage curve of the photovoltaic textile with increasing numbers of photoanode wefts connected in series. **g**, Galvanostatic charge/discharge curves at 200 mA/g (based on the active material of cathode). The battery fibre exhibited a mass capacity of 176.9 mAh/g. **h**, Schematic of the working mechanism of the energy harvesting and storing module. **i**, Photocharging and discharging curves of the battery fibre. Six photovoltaic units in series under illumination are used to charge zinc-ion battery fibres. The battery fibres are discharged to an external circuit at a current of 80 μA.

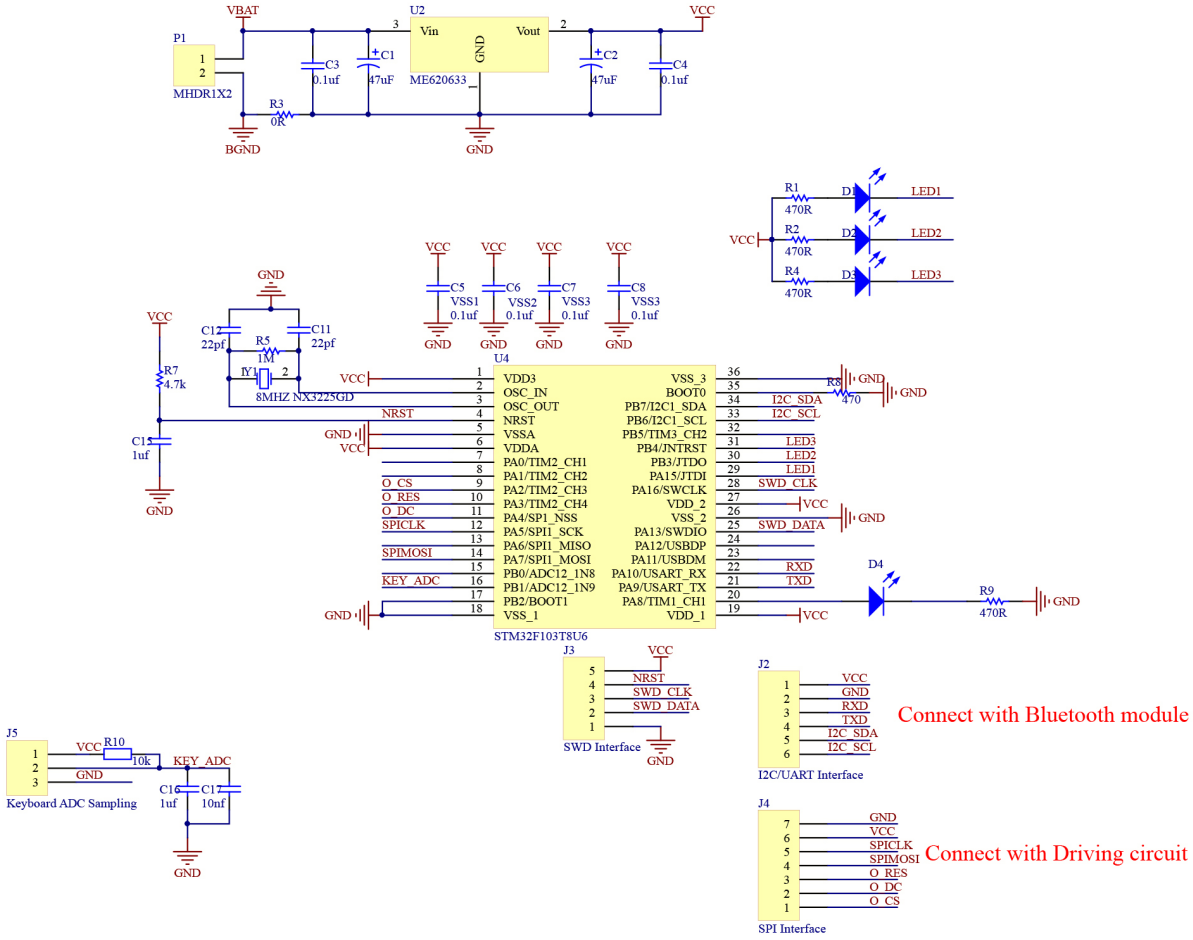

579

580

581 **Extended Data Fig. 9** | Schematic diagram of the integrated textile system.

Figures

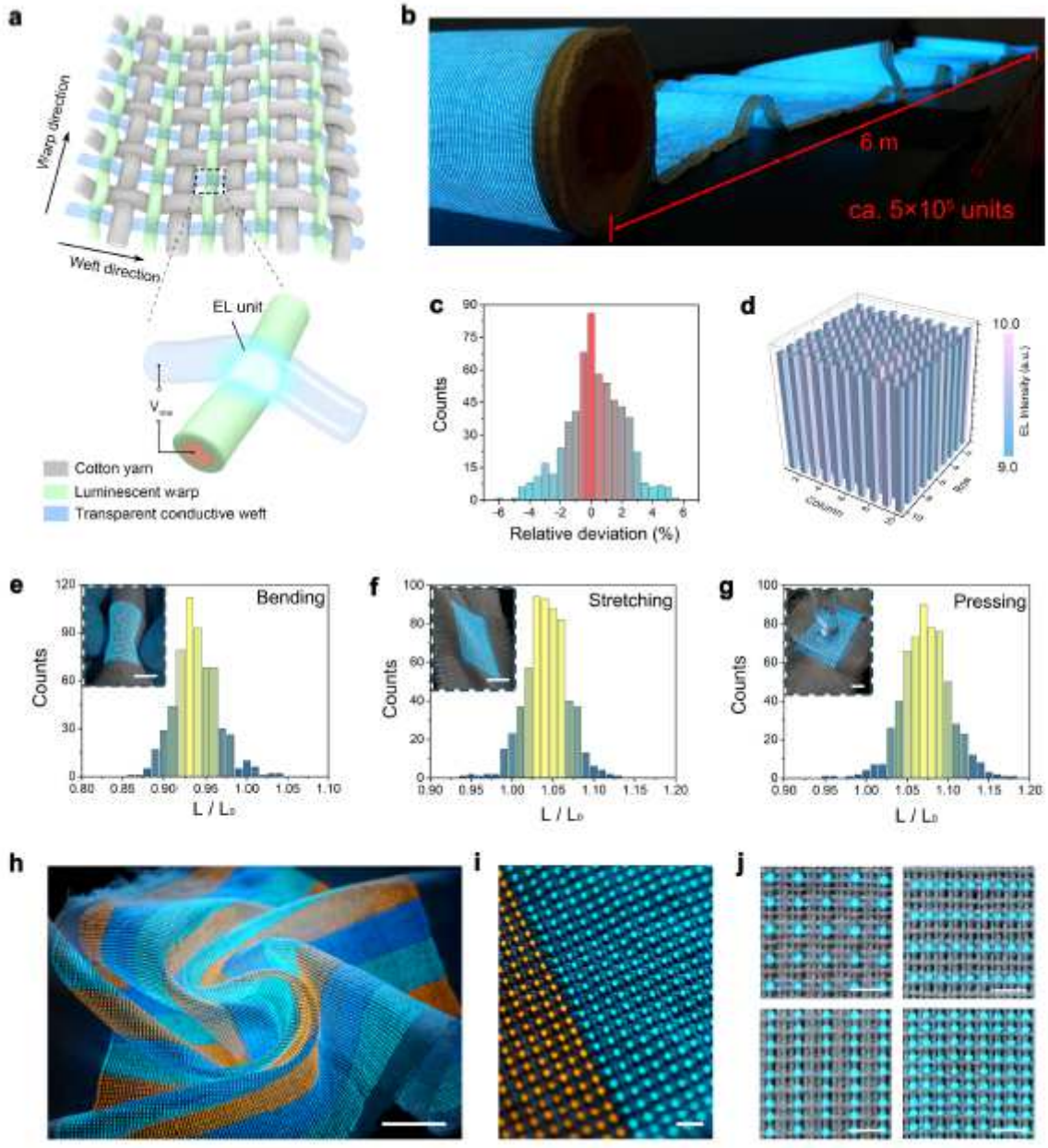

Figure 1

Structure and EL performance of the display textile. a, Schematic showing the weave diagram of the display textile. Each contacting luminescent warp and transparent conductive weft forms an EL unit (inset). Applied alternating voltage (Vrms) turns on the EL units. b, Photograph of a 6-metre-long display textile consisting of approximately 5×105 EL units. c, Statistical distribution shows the relative deviations of emission intensity for 600 EL units examined are between -6.3% and 5.2%. Relative deviation is defined as deviation of luminance for a single EL unit from the average value. d, Emission intensities of a 10×10 EL unit array is uniform (< 10% 440 differences in intensity among the units). e-g, Statistical distribution shows minor (< 10%)variations in luminance for 600 EL units after 1,000 cycles of bending (e), stretching

(f), and pressing (g). Insets: photographs of tested samples. Scale bars, 1 cm. h, Photograph of a functional multicolour display textile under complex deformations, including bending and twisting. Blue and orange are achieved by doping ZnS with copper and manganese, respectively. Scale bar, 2 cm. i, Magnified photograph of the multicolour display textile from h show EL units are uniformly spaced at a distance of ~800 μm. Scale bar, 2 mm. j, Photographs of EL units spaced at different distances obtained by changing the weaving parameters. Scale bars, 2 mm.

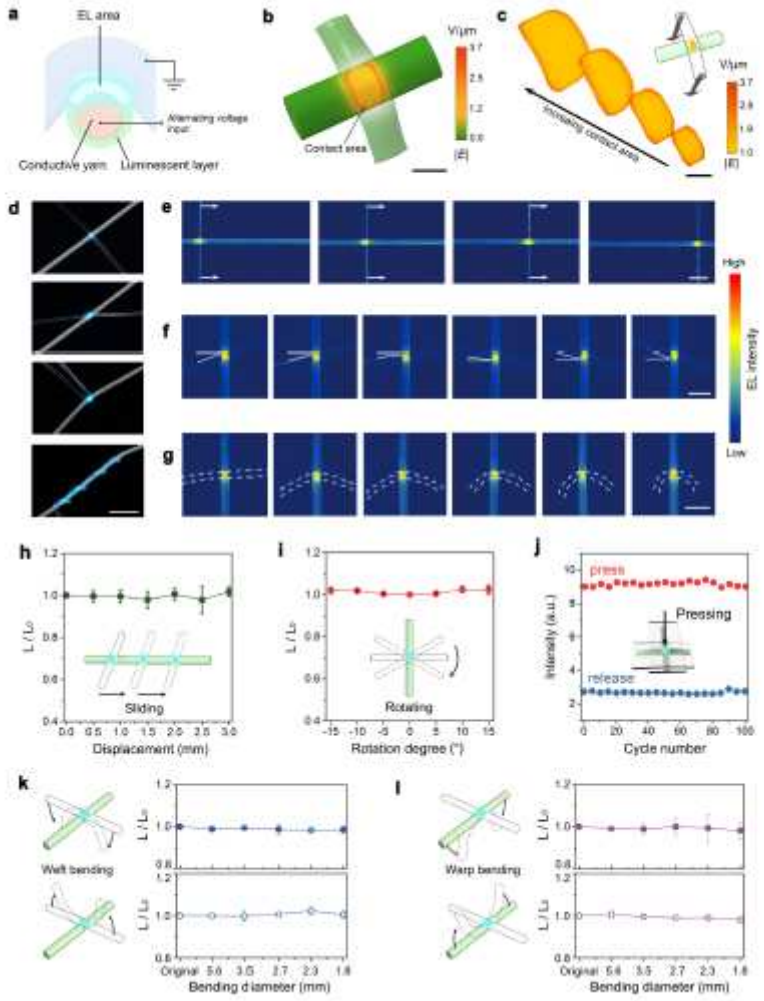

Figure 2

Characterization of EL units of the display textile. a, Schematic of an EL unit formed at the contact area between luminescent warp and transparent conductive weft. Light emission occurs when an alternating electric voltage is applied. b, c, Simulation using finite element method shows electric field distribution at the contact area in an EL unit is uniform (b) and does not change with increasing contact areas (c). d, Photographs show stable light emission as the transparent conductive weft contacted, leaned, twisted and knotted with the luminescent warp (top to bottom). Scale bar, 2 mm. e-g, EL maps show brightness of EL units remained stable even when the transparent weft is slid (e), rotated (f) and bent (g) along the luminescent warp. Colour bar indicates relative EL intensity. Scale bars, 1 mm. h-l, Luminance varied minimally when the transparent weft is moved by 3 mm along the luminescent warp (h) and rotated by

different degrees (i; 0° is when the weft is perpendicular to the warp), and when the EL unit is pressed and released for 100 cycles (j), bent along the weft length (k) and along the warp length (l) with increasing bending angles. L0 and L correspond to the EL intensity before and after deformation, respectively. Error bars are standard deviations of the results from at least three samples.

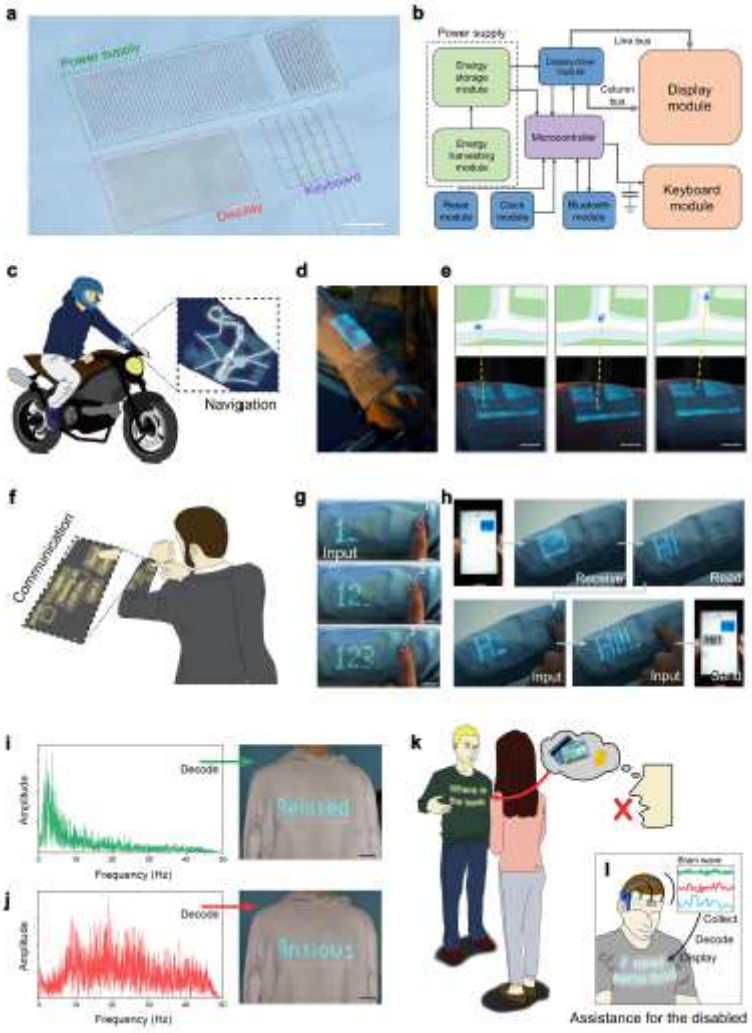

Figure 3

Application scenarios of integrated textile systems. a, Photograph of an integrated textile system consisting of display, information input (keyboard) and power supply modules. Scale bar, 2 cm. b, System-level block diagram of the integrated textile system in a shows the modules connected to a microcontroller that is powered by solar energy harvesting and electrical energy storing modules. c, Schematic illustrating the integrated textile as a smart node for the Internet of Things to offer location services during driving. Selective illumination on the display module is achieved by scanning electrical signals from the driver circuit row by row onto the array of EL units. d, e, Real-time location at a T-junction on a sleeve, transferred through the Bluetooth and microcontroller modules, is synchronized with the location map on a smartphone. Scale bars, 1 cm. f, Schematic shows textiles integrated with a display and keyboard can be used as a communication platform. g, Information is input onto clothes by pressing

the keypress that is woven into the textile. Scale bars, 2 cm. h, Receiving and sending messages between the integrated textile system and a smartphone. i, j, Expressions of mental states by decoding representative electroencephalogram signals. The words “Relaxed” (i) and “Anxious” (j) are displayed on clothes when the dominant brain waves are detected in the low-frequency region (0–10 Hz) and high-frequency region (10–40 Hz), respectively. Scale bars, 5 cm. k, Display textiles could in the future enable individuals with speech disorders to communicate and express themselves. l, Conceptual image showing brain waves from a disabled person are being decoded into messages that are displayed on a shirt made from an integrated textile.

Supplementary Files

This is a list of supplementary files associated with this preprint. Click to download.

- SupplementaryMovie1.mp4
- SupplementaryMovie2.mp4
- SupplementaryMovie3.mp4
- FigS1.png
- FigS2.png
- FigS3.png
- FigS4.png
- FigS5.png
- FigS6.png
- FigS7.png
- FigS8.png
- FigS9.png